Magnetic and hydrogen ordering in the frustrated Laves hydrides $RMn_2H_{4.5}$ (R=Y, Gd, Tb, Dy, Ho): A neutron-diffraction study

I. N. Goncharenko*
Laboratoire Léon Brillouin, CEA-CNRS CEA/Saclay, 91191 Gif sur Yvette, France and Russian Research Center ''Kurchatov Institut,'' 123182 Moscow, Russia

I. Mirebeau
Laboratoire Léon Brillouin, CEA-CNRS CEA/Saclay, 91191 Gif sur Yvette, France

A. V. Irodova
Russian Research Center ''Kurchatov Institut,'' 123182 Moscow, Russia

E. Suard
Institut Laüe Langevin, 156X, 38042 Grenoble, France
(Received 30 July 1998)

We have studied the magnetic and crystal structures of different Laves hydrides $RMn_2H_{4.5}$ (R=Y, Gd, Tb, Dy, Ho), having the cubic $C15$ structure at high temperature. We observe a strong coupling between the hydrogen and magnetic order in the frustrated Mn sublattice. The Néel temperature coincides with the ordering temperature in the hydrogen sublattice, resulting in a single magnetostructural transition. In contrast to the RMn_2 compounds, in the hydrides the Mn-Mn magnetic interaction dominates and it imposes the magnetic order in the rare-earth sublattice. On the other hand, the anisotropy of the rare-earth ion strongly influences the orientation of the magnetic moments at low temperature. The Laves hydrides show a very unusual case where the structural and magnetic orders strongly interact with each other. They also offer many examples of the interplay between the localized Mn moments and the rare-earth moments. [S0163-1829(99)13213-2]

I. INTRODUCTION

The RT_2 compounds, where R is either a rare-earth metal or yttrium, and T is a transition metal (Fe, Ni, Co, Mn), have been intensively studied for several reasons. First of all, the moments of the transition metal are close to the instability limit between localized and itinerant moments. Consequently, they become delocalized below some critical distance d_c between first neighbors T atoms.[1] In the RFe_2 family, well localized moments are observed in all compounds, whereas no magnetic moment exists for the Ni-based Laves phases. For Mn and Co compounds, the first-neighbor distances are very close to d_c. In most cases, Mn and Co atoms do not carry a magnetic moment, but it could be induced by the molecular field of the rare-earth sublattice.[1,2] Secondly, in the $C15$ structure of the cubic Laves phases, the T atoms form a pyrochlore-like sublattice, which is known as fully frustrated for first-neighbor antiferromagnetic interactions.[3] In the pyrochlore lattice, no spin arrangement minimizes the free energy, which results in a fully degenerated spin-liquid state at $T=0$ K.[4–6] Among the compounds where the transition metal carries an intrinsic moment, YMn_2 is the only one where antiferromagnetic long-range order appears in the frustrated Mn sublattice. The frustration yields a complicated helicoidal order associated with a structural distortion at the Néel transition. YMn_2 is situated very close to the limit of instability, and its unusual magnetism was intensively studied using different chemical substitutions and pressure measurements.[7–11]

Recently, the hydrides of Laves phases attracted much attention.[12–15] Hydrogen occupies the interstitial sites in the metal sublattices. It could influence the magnetic order in several ways. Firstly it expands the lattice, acting like a negative pressure, so that it could stabilize the localized moments. Secondly, it could change the magnetic interactions by modifying the electronic structure. Furthermore, it could form ordered superstructures, changing the symmetry of the surroundings of the magnetic atoms and introducing structural distortions. These points are especially important with regards to the magnetic interactions in the Mn lattice, since H order could act as a possible way to decrease the topological frustration. It is important to note that the hydrogen sublattice and the Mn magnetic sublattices are characterized by energy scales of the same order of magnitude and have about the same ordering temperature (around 300 K).

Some of the cubic RMn_2H_x (R=Y, Gd, Tb, Dy, and Ho) compounds have been studied by different techniques, like magnetic measurements,[12,13] NMR and Mössbauer spectroscopy,[14] x-ray and neutron diffraction.[15] From these data, it was concluded that H doping stabilizes local moments and increases ordering temperatures. In YMn_2H_x, depending on H concentration, the hydrides either show a ferrimagnetic behavior ($1<x<3.5$), or behave as antiferromagnets at high doping content ($x\cong 4$ to 4.5).[13] Up to very recent times, there was no detailed characterization of the long-range-ordered structures, neither in the hydrogen nor in the magnetic sublattices. Recently, the interplay between Mn and H orders was studied in detail in $YMn_2D_{4.3}$, using neutron diffraction and isotopic contrast H/D to identify magnetic and hydrogen superstructures.[16] We found that

the structural and magnetic orders have the same rhombohedral symmetry. We observed a first-order magnetostructural transition, where the magnetic sublattice changes from the paramagnetic state to an antiferromagnetic one, as the hydrogen forms an ordered superstructure.

In the present paper, we present a systematic study of all the members of the $R\mathrm{Mn_2H}_x$ family having the cubic $C15$ structure, and the maximum hydrogen content ($x = 4.1-4.5$). At this high H content, the Mn-Mn distance is well above the critical distance, so that we could expect well localized moments on Mn sites. This situation strongly differs from that in the $R\mathrm{Mn_2}$ family[1,2] where the Mn-Mn distances are about or below d_c, so that the rare-earth magnetism dominates, inducing magnetic moments on some Mn sites. Moreover in the present case, the dense H packing should strongly influence the magnetic interactions both in the Mn and in the rare-earth sublattice.

II. EXPERIMENTAL DETAILS

The starting intermetallic compounds have been prepared by arc melting from Mn of 99.99% purity and rare-earth metals with a typical of purity of 99.9%. For the Gd compound, we used the $\mathrm{Gd^{160}}$ isotope due to the huge neutron absorption of natural Gd. The hydrides (deuterides) were prepared by absorption of hydrogen (deuterium) gas at 273 K, at the pressure of 0.1–0.4 bar. For the neutron studies we used the deuterium isotope to decrease the incoherent scattering. In the following, we will speak about hydrogen, whatever isotope (H or D) was used. The hydrogen content was estimated by measuring the volume of the absorbed gas. Usually, between 1 and 3 h were needed to obtain the hydride with the maximal hydrogen content. The quality of the samples was checked by x-ray-diffraction at ambient temperature. The hydrides show narrow Bragg lines corresponding to a homogeneous hydrogen distribution within the sample. The samples are single phase, besides a small amount (of about 5%) of $\mathrm{HoD_3}$ in the Ho sample. $\mathrm{HoD_3}$ is not magnetic down to 1 K, so that its presence does not influence the analysis of the magnetic scattering.

The powder neutron-diffraction measurements have been carried out on the diffractometers D2B and D1B in ILL and G6.1 in LLB. The high-resolution diffractometer D2B (with an incident neutron wavelength of 1.593 Å) was used for the full determination of the magnetic and crystal structures. The high-flux diffractometers D1B and G6.1 (of wavelength 2.4 and 4.734 Å, respectively) allowed us to study the temperature dependence of the magnetic order in details. For the Dy and Gd samples, we used a double-cylinder sample holder to reduce the neutron absorption. Both crystal and magnetic structure data were analyzed using the FULLPROF program.[17]

III. EXPERIMENTAL RESULTS

Typical neutron-diffraction spectra are shown in Figs. 1 and 2. In all samples, we observe the same first-order magnetostructural transition around 270–350 K as found in $Y\mathrm{Mn_2D_{4.3}}$ (Ref. 16). At the transition, several phenomena occur simultaneously as the temperature decreases. First of all, we observe a strong decrease of the diffuse scattering arising from the disordered hydrogen sublattice. This scattering appears in Fig. 1(a) as a broad diffuse peak around 45 degrees. It is related with liquidlike short-range correlations and corresponds to a blocking distance between H atoms of 2.1 Å. Secondly, we observe a rhombohedral distortion of the unit cell, clearly seen by a split of the structural peaks. Moreover, new sets of diffraction peaks appear, showing a superstructure with propagation vector $\frac{1}{2}\,\frac{1}{2}\,\frac{1}{2}$. As in $Y\mathrm{Mn_2D_{4.3}}$ the transition can be described by simultaneous hydrogen and antiferromagnetic (AF) orders (with propagation vectors $\mathbf{k}=0$ and $\mathbf{k}=\frac{1}{2}\,\frac{1}{2}\,\frac{1}{2}$, respectively).

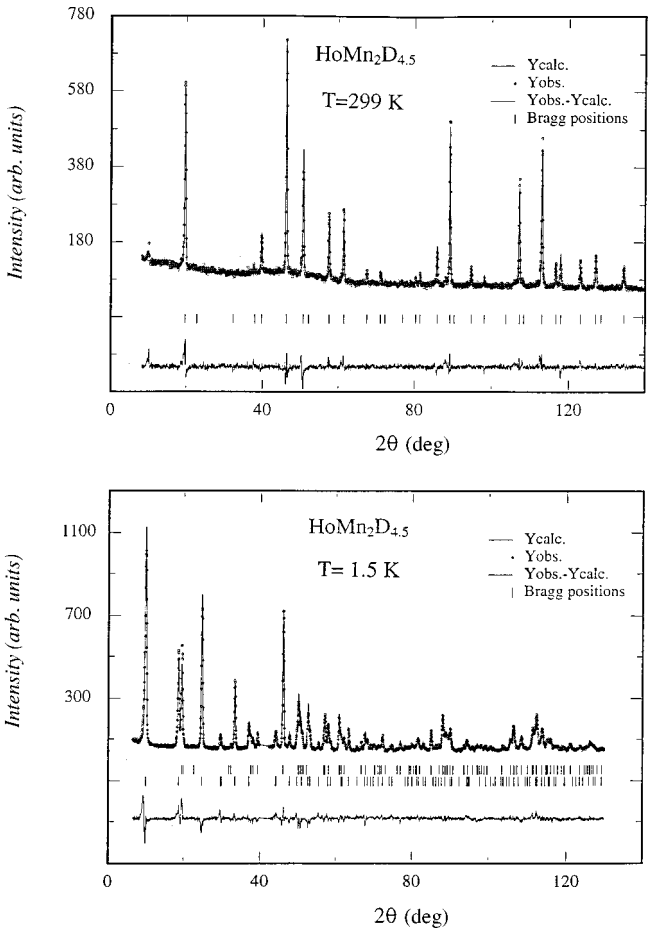

FIG. 1. Neutron-diffraction spectra measured in $\mathrm{HoMn_2D_{4.5}}$ at 299 K (above T_N) and 1.5 K with a neutron wavelength of 1.593 Å.

Above the transition, the crystal structure is described within the space group $Fd3m$, by assuming a random distribution of the 35 hydrogen atoms among the 96 g positions of the cubic unit cell (interstices $2R-2\mathrm{Mn}$). To describe the crystal structure below the transition, we used the same model as for $Y\mathrm{Mn_2D_{4.3}}$, i.e., the space group $R3m$ where hydrogen atoms occupy two kinds of positions $3b$ with occupancy 0.95 and one position $6c$ with occupancy 0.5. In all cases we get a reasonable agreement with the experimental data (R_F around 6% and R_{Bragg} below 10%). Typical refinements are shown in Figs. 1 and 2. The lattice constant and the rhombohedral angle deduced from these refinements are shown versus temperature in Fig. 3. They show an abrupt change at the Néel temperature, characteristic of a first-order transition. The Néel transition remains in the same temperature range (260–360 K) for all compounds, close to the value in $Y\mathrm{Mn_2D_{4.3}}$.

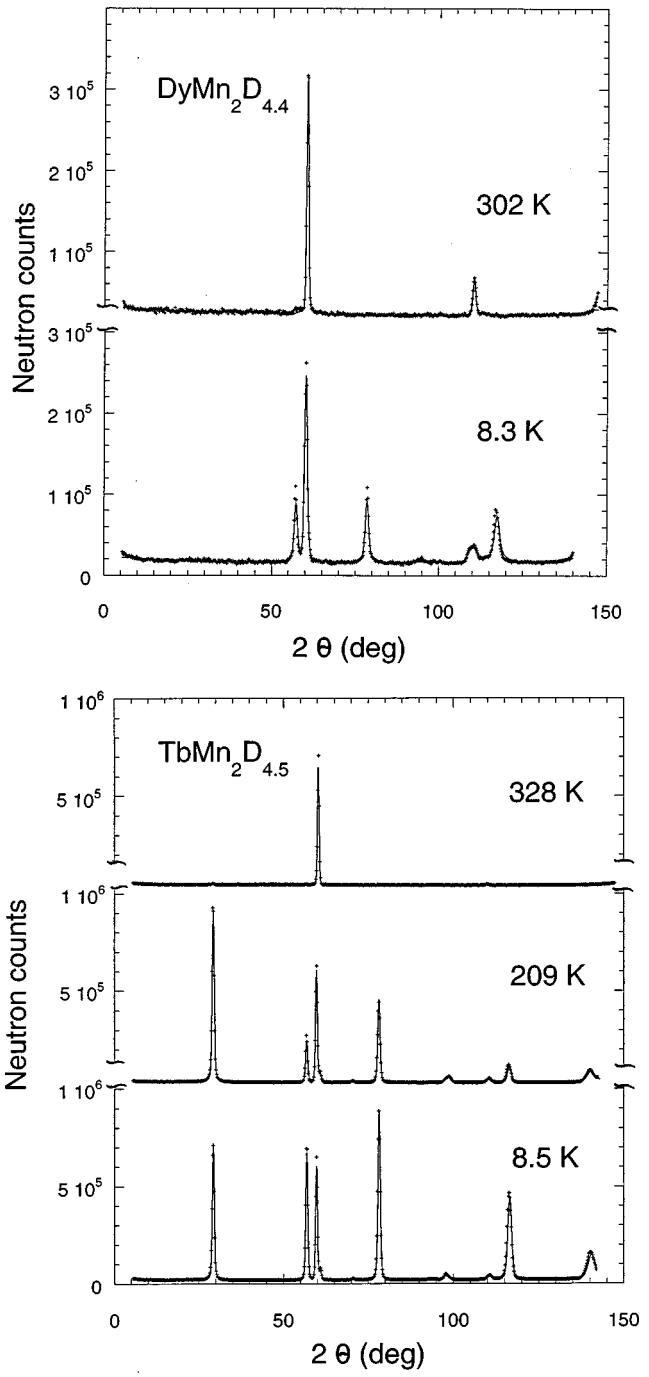

FIG. 2. Neutron-diffraction spectra measured (a) in $TbMn_2D_{4.5}$ at three temperatures: 8.5 K ($T<T_R$), 209 K ($T_R<T<T_N$), and 328 K ($T>T_N$). (b) in $DyMn_2D_{4.4}$ at two temperatures: 8.3 K ($T<T_N$) and 302 K ($T>T_N$). The neutron wavelength is 4.734 Å. Solid lines correspond to FULLPROF refinements.

In contrast with the structural peaks, the magnetic intensities and their temperature dependences (Fig. 4) show important differences with $YMn_2D_{4.3}$. First of all the $\frac{1}{2}\frac{1}{2}\frac{1}{2}$ magnetic peak, the strongest one in $YMn_2D_{4.3}$, does not exist in the Dy sample. In the Gd and Dy samples, the temperature dependence of the magnetic intensities is monotonic, like in $YMn_2D_{4.3}$, whereas for Tb and Ho the intensity of the $\frac{1}{2}\frac{1}{2}\frac{1}{2}$ peaks decreases abruptly at some intermediate temperature. Since in all cases the magnetic peaks are indexed with the propagation vector $\frac{1}{2}\frac{1}{2}\frac{1}{2}$, we conclude that the temperature behaviors of the magnetic intensities should be associated either with a reorientation of the magnetic moments, or with some interplay between the temperature dependence of the Mn and rare-earth moments. In order to describe the experimental data, we made a systematical search among the different models of spin orientation within the high-symmetry directions. We tried collinear Mn and R sublattices as well as some noncollinear arrangements. The results are summarized in Table I. The final models give a good agreement with the experimental data for all samples in the whole temperature range ($R_{\text{magn}}<10\%$). The temperature dependences of the magnetic moments obtained by FULLPROF are shown in Fig. 5. In all samples we found collinear arrangements of R and Mn spins, which order simultaneously at T_N. The Gd sample could be described by the same model as the Y sample, i.e., all moments lying in the plane perpendicular to the [1 1 1] direction. In the Dy sample, the magnetic moments are parallel to the [1 1 1] direction. This explains why we do not observe the $\frac{1}{2}\frac{1}{2}\frac{1}{2}$ reflection. In both Gd and Dy samples the direction of magnetic moments does not change with temperature. In contrast, we found a reorientation transition in the Tb and Ho samples, where the magnetic structure which takes place just below T_N is the same as in $YMn_2D_{4.3}$ and Gd samples. At some intermediate temperature T_R the magnetic moments reorient to the direction [1 0 0] and [1 −1 1] in the Tb and Ho samples, respectively. The reorientation transitions are sharp and the Mn and R magnetic moments remain collinear throughout the transition. The magnitude of the magnetic moments does not change at T_R. The Mn moment saturates rather quickly below T_N whereas the rare-earth moment increases smoothly down to the lowest temperature, approaching the value of the free Gd, Tb, and Ho ions ($gJ=7$, 9, and $10\mu_B$, respectively). Only in the Dy sample does the moment at low temperature remain significantly smaller than the free-ion value ($gJ=10\mu_B$).

The rhombohedral unit cell contains two R atoms occupying two positions $1a$, and four Mn atoms with positions $1a$ and $3b$ of the space group $R3m$. The magnitude of the magnetic moments at the various sites, [as called $R1$, $R2$, Mn(1) and Mn(2) in the following], are not necessarily the same. Nevertheless, our fits do not show significant differences between the magnetic moments corresponding to nonequivalent positions both in R and in Mn sublattices. In Fig. 5 we present results assuming only one R moment and two different moments at Mn $1a$ and Mn $3b$ sites [Mn(1) and Mn(2), respectively]. Although in the Tb and Ho samples, the Mn(1) moments seem to be systematically smaller than the Mn(2) ones, the difference does not go far from the experimental error. In the Dy sample, the high absorption of Dy increases both statistical and systematical error, and we have constrained Mn(1) and Mn(2) moments to the same value. Figure 6 shows the resulting magnetic structures of $RMn_2D_{4.3}$. The R and Mn ferromagnetic (111) planes $R1$ Mn(1) $R2$ Mn(2)-$R1$ Mn(1) $R2$ Mn(2)-$R1$ Mn(1) $R2$ Mn(2)-... are ordered in the $++--$ sequence for each type of magnetic atom (R or Mn), leading to the following packing ↑↓↑↑-↓↑↓↓-↑↓↑↑-↓↑↓↓-↑↓↑↑-↓↑↓↓ along the [1 1 1] axis, where ↑ and ↑ correspond to R and Mn moments, respectively. A schematic drawing of the magnetic structure is shown in Fig. 6.

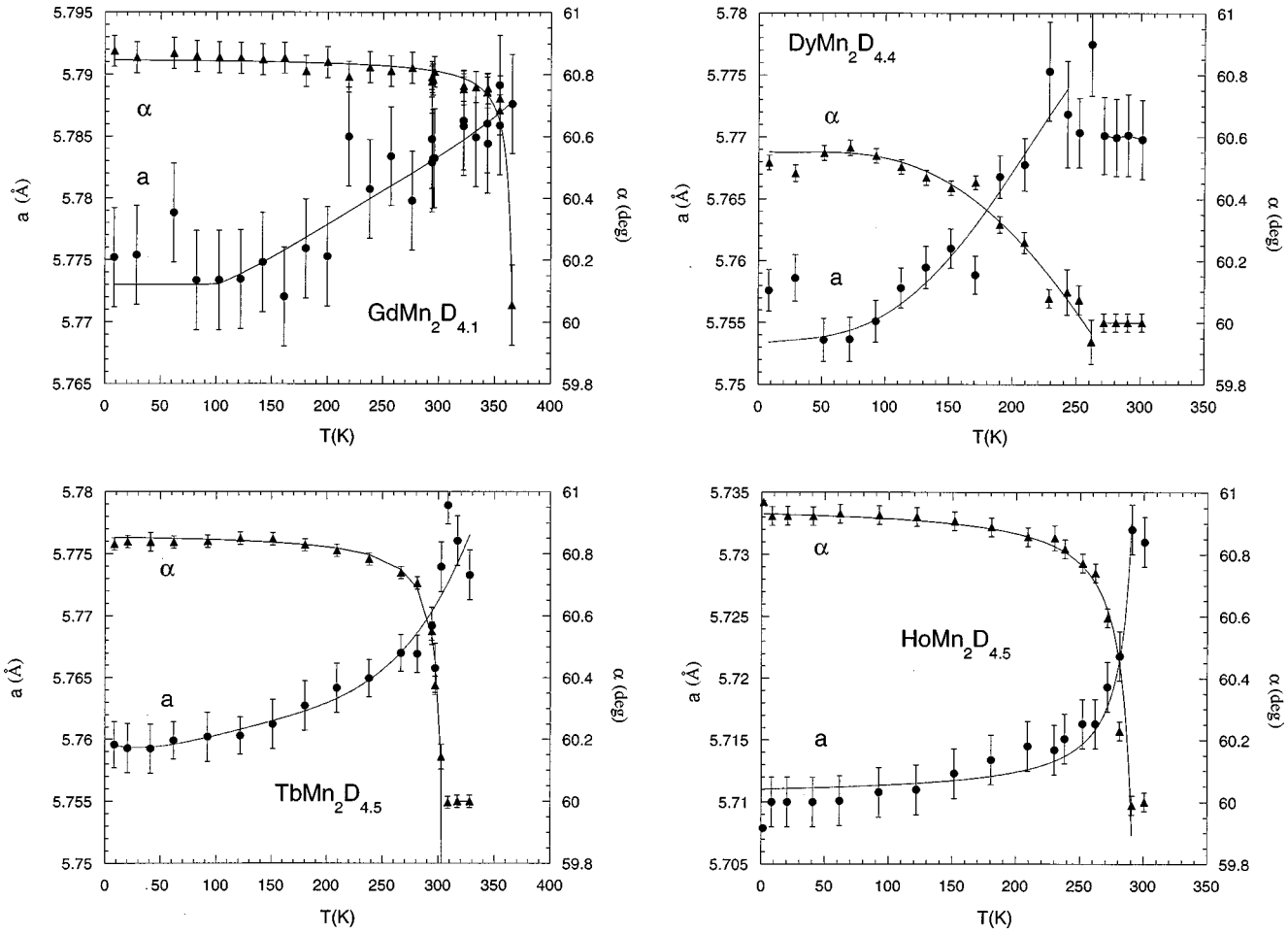

FIG. 3. Lattice constant a (Å) and rhombohedral angle α (deg) versus temperature T in the $R\mathrm{Mn_2D}_x$ family. Error bars are the standard deviations given by FULLPROF refinement. Solid lines are guides to the eye.

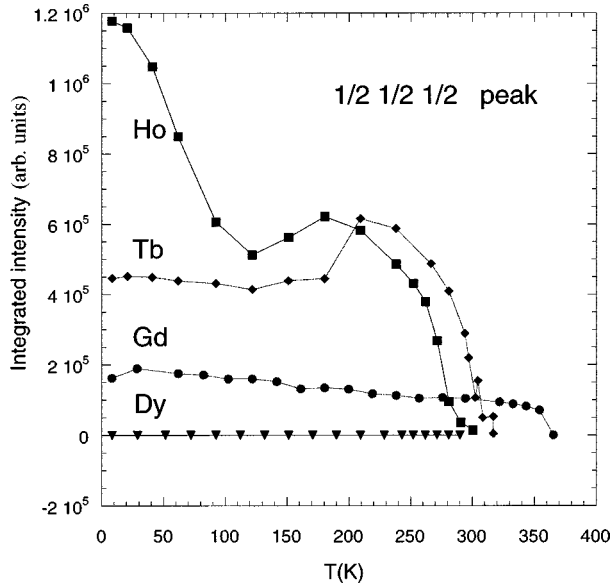

FIG. 4. Integrated intensity of the $\frac{1}{2}\ \frac{1}{2}\ \frac{1}{2}$ peak versus temperature. Solid lines are guides to the eye.

IV. DISCUSSION

In order to analyze the magnetic order, we must consider both Mn and R sublattices. In the general case, we have to consider the Mn-Mn, R-Mn, and R-R exchange interactions altogether:

$$H = H_{\text{Mn-Mn}} + H_{R\text{-Mn}} + H_{R\text{-}R}. \tag{1}$$

In the $R\mathrm{Mn_2}$ compounds, the interactions involve mostly first-neighbor exchange, mediated by d orbitals of Mn and the outer $5d$ shell of the rare earth (through intra-atomic $4f$-$5d$ exchange). Then we note that the type of magnetic order, with a propagation vector $\frac{1}{2}\ \frac{1}{2}\ \frac{1}{2}$, remains the same in $\mathrm{YMn_2D_{4.3}}$ and in the rare-earth compounds. Moreover, the ordering temperature does not change significantly by replacing Y with a magnetic rare-earth atom. It means that the contribution of $H_{\text{Mn-Mn}}$ is predominant. So we first discuss the magnetic interaction in the Mn sublattice ($H_{\text{Mn-Mn}}$) without any influence of the rare-earth magnetism.

A. Magnetic interactions in the Mn sublattice

If we consider the piling of the Mn layers perpendicular to the [1 1 1] axes, we see that the Mn(2) sites form a sequence of *kagomé* planes alternating with the hexagonal layers of the Mn(1) sites (Figs. 6 and 7). Each Mn(2) atom has six nearest Mn neighbors. Four of them belong to the same Mn(2) plane

TABLE I. Néel temperature T_N, reorientation temperature T_R, spin directions and low-temperature values of the magnetic moments in the $R\mathrm{Mn_2D}_x$ family. R_{magn} is the magnetic reliability factor obtained in the FULLPROF refinement.

Chemical formula	T_N (K)	T_R (K)	Direction of magnetic moments		Magnetic moments at 8.5 K (μ_B)			R_{magn} (%)
			$T<T_R$	$T_R<T$	R	Mn(1)	Mn(2)	
$GdMn_2D_{4.1}$	358		[−2 1 1]	[−2 1 1]	7.5(7)	3.3(5)	3.4(3)	6.6
$TbMn_2D_{4.5}$	300	180	[1 0 0]	[−2 1 1]	9.0(5)	3.6(4)	2.8(3)	3.3
$DyMn_2D_{4.4}$	265		[1 1 1]	[1 1 1]	7.7(10)	3.8(5)	3.5(3)	6.6
$HoMn_2D_{4.5}$	280	160	[1 1 −1]	[−2 1 1]	8.7(5)	3.9(5)	3.5(3)	7.6

(top of Fig. 7), whereas the remaining two belong to the two neighboring Mn(1) planes. In contrast, the Mn(1) atoms have no nearest neighbors inside the Mn(1) plane. Each Mn(1) atom has three nearest neighbors in the Mn(2) plane above and three Mn(2) nearest neighbors in the plane below (bottom of Fig. 7). The wave vector $\frac{1}{2}\ \frac{1}{2}\ \frac{1}{2}$ corresponds to the stacking sequence $++--$ of ferromagnetic (1 1 1) planes. It is easy to see that the observed magnetic structure cannot be explained by considering only first-neighbor isotropic Mn-Mn interactions. As noticed in the Introduction, the pyrochlore lattice is fully frustrated to AF first-neighbor interactions and ferromagnetic Mn-Mn interactions should yield a casual ferromagnetic order (like in YFe_2). The problem cannot be solved simply by involving the rhombohedral distortion. As discussed above, the Mn(1) atoms have nearest neighbors only in the neighboring Mn(2) planes. Since in the magnetic structure, the magnetic moments in these Mn(2) planes are antiparallel, the resulting interaction on the Mn(1)

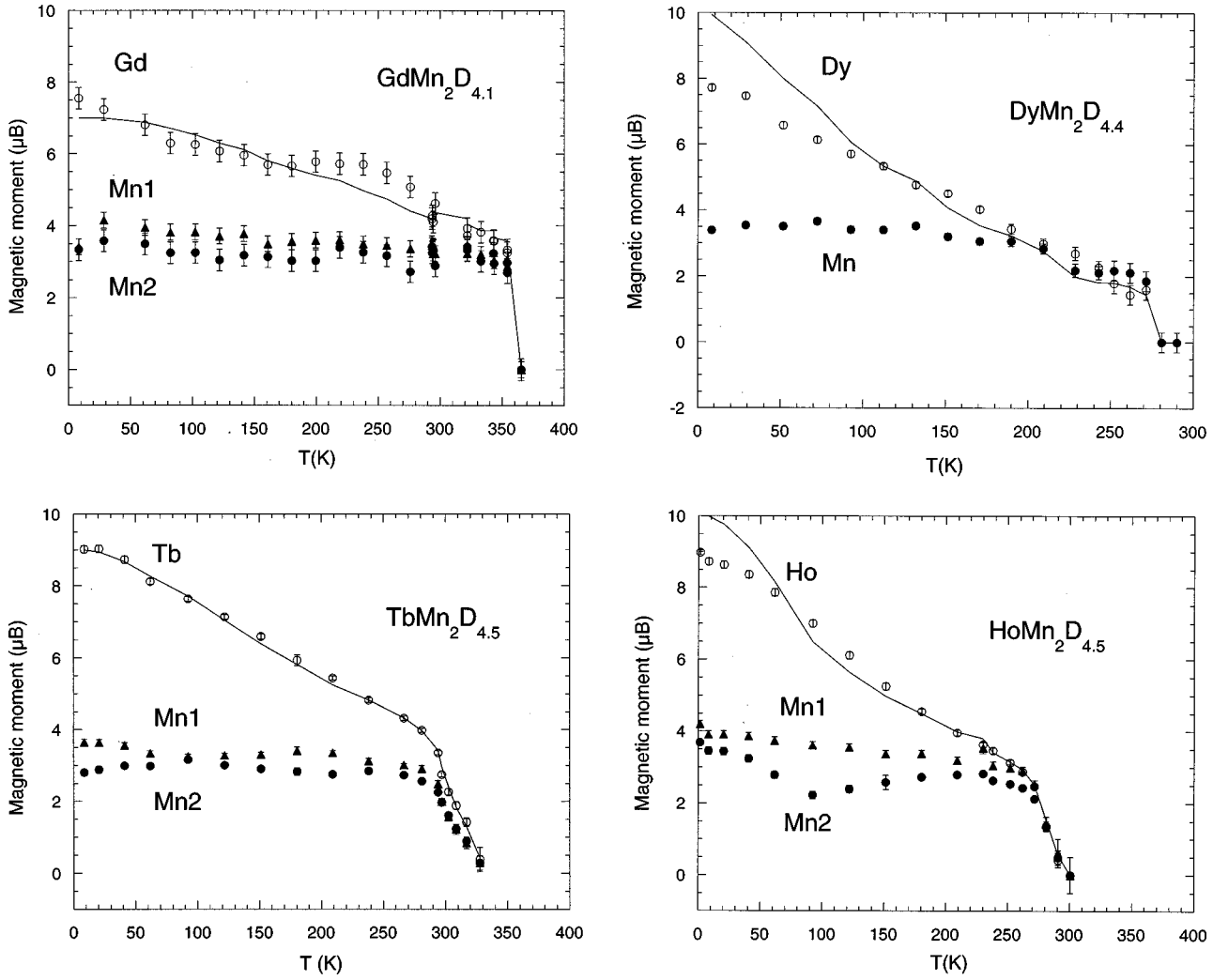

FIG. 5. Temperature dependences of the magnetic moments in the $R\mathrm{Mn_2D}_x$ family. (○) rare-earth moment. (▲) Mn(1) moment; (●) Mn(2) moment. Error bars are the standard deviations given by FULLPROF refinement. Solid line are fits of the rare-earth moment according to Eq. (2).

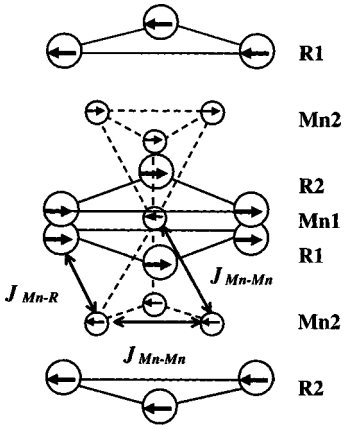

FIG. 6. Schematic drawing of the magnetic sublattices in the $R\mathrm{Mn_2D}_x$ family. The spin orientation corresponds to the Gd sample.

site should be zero for any direction of the magnetic moments in the Mn(1) plane. The rhombohedral distortion could make the Mn-Mn interaction in-plane and out-of-plane nonequivalent, but it will not affect the cancellation of the interactions on the Mn(1) site, since these interactions have the same symmetry regarding the axis of the rhombohedral distortion. The only way to make Mn-Mn interactions nonequivalent is to consider the influence of hydrogen order. Since hydrogen order decreases the symmetry of the crystal structure to $R3m$, the hydrogen sublattice is not symmetric

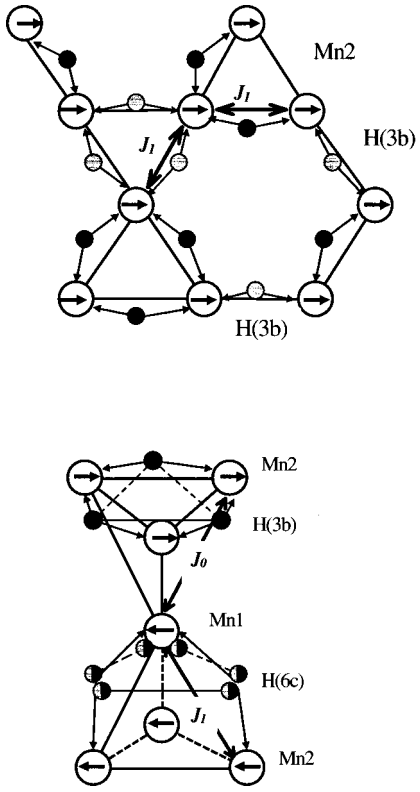

FIG. 7. Hydrogen and Mn environment of the Mn atoms. The first-neighbor surrounding in the Mn(2) (*kagomé*) plane is shown at the top. The first-neighbor surrounding of the Mn(1) atom is shown at the bottom. The black, gray, and half filled symbols correspond to the 3*b* in-plane, 3*b* out-of-plane, and 6*c* half-filled positions of the hydrogen atoms, respectively.

with respect to an inversion of the [1 1 1] axis. The details of the hydrogen surrounding are shown in Fig. 7. Each Mn-Mn couple could form two 2Mn-2Y tetrahedra. Hydrogen could occupy one or none of them, but it cannot occupy two, since the H-H distance would be smaller than 2 Å. In the ordered structure, each Mn(2)-Mn(2) couple in the Mn(2) plane has one hydrogen neighbor at the shortest Mn-H distance. Therefore, we could expect that all Mn(2)-Mn(2) interactions in the plane will be the same. In contrast, the interactions between the Mn(1) and Mn(2) planes are strongly anisotropic. The couples consisting of one Mn(1) atom and one Mn(2) atom in the plane ''down'' also have one H neighbor, whereas the couples Mn(1)-Mn(2) (up) have not. In order to describe the observed structure, we only need to assume that Mn-Mn interactions involving one H neighbor are ferromagnetic ($J_1>0$), whereas Mn-Mn interactions ''without H'' are antiferromagnetic ($J_0<0$), like in the YMn_2 compound. Consequently, the in-plane Mn interaction is ferromagnetic, whereas the out-of-plane interactions could be either ferromagnetic or antiferromagnetic.

The total energy, $H=-\Sigma \mathrm{J}_{ij}S_iS_j$ per unit cell is expressed as $H=S^2([3J_1-3J_0]+3[5J_1-J_0])$ for the $++--$ stacking sequence, assuming the same magnitude of magnetic moments at all sites. The first term corresponds to the summation over the first neighbors of the Mn(1) site, and the second term is the summation over the neighbors of the three Mn(2) sites of the unit cell. Obviously, the above spin arrangement corresponds to the minimal possible energy value when $J_1<0$ and $J_0>0$.

B. Magnetic interactions in the rare-earth sublattice

From above, we conclude that Mn-Mn interaction is predominant. To describe the magnetic order in the rare-earth sublattice, we need to consider *R*-Mn and *R*-*R* interactions. Depending on the respective strengths of these two interactions, we should expect different magnetic behaviors. If the *R*-*R* interaction was much stronger than the *R*-Mn one, the Mn and *R* sublattices could order independently with different ordering temperatures. With respect to the situation in the RT_2 compounds where *T* is nonmagnetic, we could expect that the order in the *R* sublattice will occur at a much lower temperature than in the present case. Our results show that both *R* and Mn sublattices order simultaneously. This suggests that *R*-Mn interactions are strong and likely dominate *R*-*R* interactions. In this case we can describe the magnetic order in the *R* sublattice as an ordering of the *R* moments in the molecular field of the Mn sublattice, neglecting any influence of the rare earth on the Mn sublattice (besides the direction of the magnetic moments, which will be discussed later). The ordered *R* moment could be considered as a free localized moment in the exchange field of the Mn sublattice. The energy of the J state of the magnetic rare-earth ion could be written as follows:

$$E_{\mathrm{J}}=-\sum_i J^i_{R\text{-}\mathrm{Mn}}S^{\mathrm{Mn}}S^R_{\mathrm{J}}=-2J_{R\text{-}\mathrm{Mn}}(g_{\mathrm{J}}-1)\mathrm{J}\mu_B M^{\mathrm{Mn}}, \quad (2)$$

where M^{Mn} and $J_{R\text{-}\mathrm{Mn}}$ are the ordered Mn moment and the effective exchange constant derived from the sum over *i*-Mn atoms. J is the quantum number and g_{J} is the Landé factor.

The temperature dependence of the rare-earth-ordered moment is calculated through the partition function:

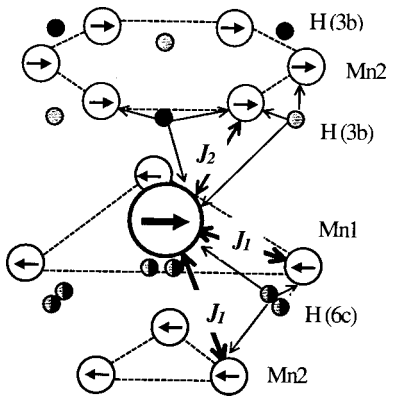

FIG. 8. Hydrogen and Mn environment of a rare-earth atom ($R2$). The black, gray, and half filled symbols correspond to the $3b$ in-plane, $3b$ out-of-plane, and $6c$ half-filled positions of the hydrogen atoms, respectively.

$$\mu^R=\left[\sum_{\mathrm{J}} g_{\mathrm{J}}\mu_B \mathrm{J}\exp(-E_{\mathrm{J}}/kT)\right]\Big/\left[\sum_{\mathrm{J}} \exp(-E_{\mathrm{J}}/kT)\right]. \tag{3}$$

We have fitted the temperature dependences of the R moments using the above formulas, taking the experimental data for the Mn-ordered moments and adjusting the effective exchange constant $J_{R\text{-Mn}}$ for each rare earth. As shown in Fig. 5 we obtain good fits, which reproduce the characteristic features of the measured temperature dependences. We find very similar values of the $J_{R\text{-Mn}}$ for the different rare-earth atoms, namely 23.2, 22.4, 19.1, and 21.1 $k\mu_B^{-2}$ for Gd, Tb, Dy, and Ho, respectively. From the temperature dependences we cannot conclude about the sign of the exchange interaction. The saturated moments obtained with this model are close to the free-ion moments, except for the Dy sample.

In order to discuss the microscopic origin of the exchange between Mn and R sublattices, we need to consider the surrounding of the rare-earth atoms. Each R atom has 12 Mn neighbors. Six of them belong to the closest Mn(2) plane, three to the Mn(1) plane, and the remaining three to another Mn(2) plane (Fig. 8). We immediately notice that the observed $++--$ stacking of the ferromagnetic Mn planes (Fig. 6) leads to nonequivalent effective interaction on the two R sites, if we consider the Mn-R interactions as isotropic ones. One of the two rare-earth sites will have nine Mn first neighbors with the same direction of magnetic moments (and opposite to the rare-earth moment) whereas another site will have six neighbors in one direction and six neighbors in the opposite direction. Consequently, for half of the rare-earth atoms the R-Mn interactions should cancel, and we should expect these atoms to remain paramagnetic, in contradiction with the experimental data. When fitting the moments on the two rare-earth sites independently, we never get a difference larger than 20%. The most significant difference is observed at the reorientation point and close to the Néel temperature and could be associated with experimental errors (when the R moments are small or not fully reoriented). Possible sources of the anisotropy of the R-Mn interactions could be the distortion of the unit cell (making the R-Mn distances different for about 1%) and the hydrogen order. If we consider the hydrogen surrounding of the R-Mn pairs in the same way as for the Mn sublattice, we see that some of the R-Mn links have two hydrogen neighbors and some only one (Fig. 8). Assuming that R-Mn interactions are AF (like in $R\mathrm{Fe}_2$), but that hydrogen neighbors increase the ferromagnetic contribution to the exchange interaction (as for Mn-Mn exchange), we can explain the magnetic order in the R sublattice. If J_1 is the R-Mn exchange interaction modified by one H neighbor and J_2 is the interaction involving two H neighbors, the resulting interaction on the two R sites is written as

$$J(R1)=-3J_1+3J_1+6J_2=6J_2,$$

$$J(R2)=-6J_2+3J_1+3J_1=-6J_2+6J_1. \tag{4}$$

Assuming that $J_1, J_2<0$ and $J_2=\frac{1}{2}J_1$, we get $J(R1)=J(R2)=3J_1$, showing that the anisotropy of the H surrounding may modify the R-Mn exchange enough to induce similar moments on the two R sites.

C. Reorientation transitions

In the above description, we considered only the stacking sequence of the moments but still did not consider their orientation with respect to the crystallographic axis. The Heisenberg Hamiltonian written above is degenerated with respect to all orientations of the magnetic lattice. The presence of spin reorientations shows that we need to consider anisotropic terms in the magnetic interactions. Since reorientation transitions occur at low temperature and the orientation depends on the nature of the rare earth, it is natural to expect that the orientation at $T=0$ K is controlled by the rare-earth anisotropy. On the other hand, besides the Dy sample the direction of the magnetic moments in the high-temperature phase is the same in all samples, and it coincides with that in $\mathrm{YMn_2D_{4.3}}$. This suggests that in the temperature range $T_R<T<T_N$ the spin orientation is governed by Mn anisotropy. The simplest way to involve anisotropy is to write the Hamiltonian as

$$H=H_{\mathrm{isotrop}}+H_{\mathrm{anisot}}=\{H_{\text{Mn-Mn}}+H_{R\text{-Mn}}\}+F_R+F_{\mathrm{Mn}}, \tag{5}$$

where F_R and F_{Mn} are the anisotropic terms for the R and Mn sublattices, respectively. For the rare earth the crystal field is supposed to be the main origin of the anisotropy. In the cubic structure F_R may be written as $F_R=V_4+V_6$ where V_4 and V_6 are the fourth- and six-order terms of the crystal field.[18] When considering only the fourth term, the energy is minimized for the directions of [1 0 0], [1 1 0] or [1 1 1], depending on the type of rare earth and on the crystal-field parameters.[19] The above directions in the cubic cell correspond to the directions [1 −1 1], [1 0 0], and [1 1 1] of the rhombohedral unit cell, i.e., the directions observed in Ho, Tb, and Dy samples, respectively, at $T<T_R$ (Fig. 9).

A reorientation transition may be expected since the Mn-ordered moments saturate very rapidly below T_N, whereas the rare-earth moments continue to increase with decreasing temperature. Consequently the balance between F_R and F_{Mn} may change at some temperature, resulting in the reorientation transition. If the rare-earth anisotropy is mostly due to crystal field, no reorientation should be expected in the Gd sample, since the moment of the Gd^{3+} ion has only a spin

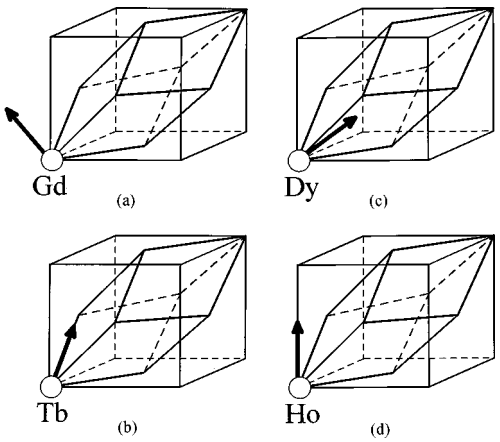

FIG. 9. Spin orientations at low temperature in the $R\mathrm{Mn_2D}_x$ family, as shown with respect to the rhombohedral and the cubic unit cell.

component. In the Dy sample, the anisotropy of the Dy ion is strong enough to orient the moments already at T_N.

The above situation may be compared with that in $R\mathrm{Fe}_2$ compounds.[19–21] In both $R\mathrm{Mn_2D}_{4.3}$ and $R\mathrm{Fe}_2$ systems, stable moments exist on the transition metals T, the R-T interactions are much smaller than the T-T ones, and the R-R interactions are negligible. However, in the $R\mathrm{Fe}_2$ compounds ferrimagnetic structures are observed, the spin directions are imposed by the R anisotropy up to the Néel temperature, and the Fe anisotropy only induces small shifts in the boundaries of the spin orientation diagrams.[19] In our case, the influence of the anisotropy of the transition metal seems to be much stronger.

V. CONCLUSION

We have observed a strong coupling between rare earth and Mn sublattices. The two sublattices order at the same temperature and remain collinear through the reorientation transition. The behavior of the R moments is rather different from that in $R\mathrm{Mn}_2$ compounds, where the coupling between R and Mn sublattices is ferromagnetic. It seems to be much closer to the behavior in $R\mathrm{Fe}_2$ systems, having well localized Fe moments. Both in $R\mathrm{Fe}_2$ and $R\mathrm{Mn_2D}_{4.3}$ the coupling between the R and T sublattices is antiferromagnetic. However, in $R\mathrm{Mn_2D}_{4.3}$ the order inside each sublattice is antiferromagnetic whereas in $R\mathrm{Fe}_2$ it is ferromagnetic.

Therefore, the studied Laves hydrides represent a very interesting case when Mn drives a simple long-range antiferromagnetic order in a pyrochlore-like sublattice. The results can be explained only by involving the mutual influences of hydrogen and magnetic orders which release the frustration.

ACKNOWLEDGMENTS

We appreciate the contribution of A. S. Markosyan in the preparation of the starting GdMn_2 compound. We also thank R. V. Gladkich and G. V. Laskova for their help in the sample preparation and x-ray experiments. This work was partly supported by the Russian foundation for Basic Research, Grant No. 96-02-19775 and the Russian State Program ''Neutron Investigations of Condensed Matter.''

*Author to whom correspondence should be sent; electronic address: gonch@llb.saclay.cea.fr

[1] M. Shiga, Physica B **149**, 293 (1988); J. Magn. Magn. Mater. **129**, 17 (1994).

[2] C. Ritter, R. Cywinski, S. H. Kilkoyne, and S. Mondal, J. Phys.: Condens. Matter **4**, 1559 (1992); C. Ritter, R. Cywinski, S. H. Kilkoyne, S. Mondal, and B. D. Rainford, Phys. Rev. B **50**, 9894 (1994); R. Z. Levitin and A. S. Markosyan, J. Magn. Magn. Mater. **177-181**, 563 (1998).

[3] R. Ballou, J. Deportes, R. Lemaire, and B. Ouladdiaf, J. Appl. Phys. **63**, 3487 (1988); R. Ballou, C. Lacroix, and M. D. Nunez-Regueiro, Phys. Rev. Lett. **66**, 1910 (1991).

[4] J. Villain, Z. Phys. B **33**, 31 (1978).

[5] J. N. Reimers, Phys. Rev. B **45**, 7287 (1992).

[6] B. Canals and C. Lacroix, Phys. Rev. Lett. **80**, 2933 (1998).

[7] R. Ballou, J. Deportes, R. Lemaire, Y. Nakamura, and B. Ouladiaff, J. Magn. Magn. Mater. **70**, 129 (1987); R. Ballou, E. Lelièvre-Berna, and B. Fak, Phys. Rev. Lett. **76**, 2125 (1996).

[8] R. Cywinski, S. H. Kilkoyne, and C. A. Scott, J. Phys.: Condens. Matter **3**, 6473 (1991); B. D. Rainford, S. Dakin, and R. Cywinski, J. Magn. Magn. Mater. **104-107**, 1257 (1992).

[9] G. M. Kalvius, Hyperfine Interact. **84**, 249 (1994).

[10] I. S. Dubenko, E. Gratz, A. Lindbaum, A. S. Markosyan, S. A. Markossian, V. E. Rodimin, and G. Wiesinger, J. Magn. Magn. Mater. **177-181**, 571 (1998).

[11] R. Hauser, E. Bauer, E. Gratz, Th. Hauffer, G. Hilsher, and G. Wiesinger, Phys. Rev. B **50**, 13 493 (1994); S. Mondal, R. Cywinski, S. H. Kilkoyne, B. D. Rainford, and C. Ritter, Physica B **180-181**, 108 (1992).

[12] K. H. J. Bushow and R. C. Sherwood, J. Appl. Phys. **48**, 4643 (1977).

[13] H. Fuji, M. Saga, and T. Okamoto, J. Less-Common Met. **130**, 25 (1987).

[14] J. Przewoznik, J. Zukrowski, and K. Krop, J. Magn. Magn. Mater. **140-144**, 807 (1995); Cz. Kapusta, J. Przewoznik, J. Zukrowski, H. Figiel, J. S. Lord, P. C. Riedi, V. Paul-Boncour, M. Latroche, and A. Percheron-Guegan, Phys. Rev. B **54**, 14 922 (1996).

[15] J. Przewoznik, V. Paul-Boncour, M. Latroche, and A. Percheron Guegan, J. Alloys Compd. **232**, 107 (1996); M. Latroche, V. Paul-Boncour, J. Przewoznik, A. Percheron-Guegan, and F. Bourée-Vigneron, *ibid.* **231**, 99 (1995).

[16] I. N. Goncharenko, I. Mirebeau, A. V. Irodova, and E. Suard, Phys. Rev. B **56**, 2580 (1997); I. Mirebeau, I. Goncharenko, A. V. Irodova, and E. Suard, Physica B **241-243**, 672 (1998).

[17] J. Rodriguez-Carvajal, Physica B **192**, 55 (1993).

[18] K. R. Lea, M. J. M. Leask, and W. P. Wolf, J. Phys. Chem. Solids **23**, 1381 (1962).

[19] U. Atzimony, M. P. Dariel, E. R. Bauminger, D. Lebenbaum, I. Nowik, and S. Ofer, Phys. Rev. Lett. **28**, 244 (1972); Phys. Rev. B **7**, 4220 (1973).

[20] J. J. Rhyne, J. Magn. Magn. Mater. **70**, 88 (1987).

[21] M. S. S. Brook, L. Nordström, and B. Johansson, J. Phys.: Condens. Matter **3**, 2357 (1991); M. S. S. Brook, T. Gasche, S. Auluck, L. Nordström, L. Severin, J. Trygg, and B. Johansson, J. Appl. Phys. **70**, 5972 (1991).